CHANS-SD-YRB V1.0: A System Dynamics model of the coupled human-natural systems for the Yellow River Basin

Shan Sang[1,2], Yan Li[1,2*], Shuang Zong[1,2], Lu Yu[1,2], Shuai Wang[1,2], Yanxu Liu[1,2], Xutong Wu[1,2], Shuang Song[1,2], Wenwu Zhao[1,2], Xuhui Wang[3], Bojie Fu[4]

[1]State Key Laboratory of Earth Surface Processes and Hazards Risk Governance (ESPHR), Beijing Normal University, Beijing, China

[2]Institute of Land Surface System and Sustainable Development, Faculty of Geographical Science, Beijing Normal University, Beijing, China

[3]Institute of Carbon Neutrality, Laboratory for Earth Surface Processes, College of Urban and Environmental Sciences, Peking University, Beijing 100871, China

[4]State Key Laboratory of Regional and Urban Ecology, Research Center for Eco-Environmental Sciences, Chinese Academy of Sciences, Beijing 100085, China

Corresponding Author:

Yan Li, Ph.D.

Institute of Land Surface System and Sustainable Development, Faculty of Geographical Science, Beijing Normal University, Beijing, 100875, China

Email: yanli.geo@gmail.com

Abstract: Modeling the coupled human–natural systems (CHANS) is vital for understanding human–natural interactions and achieving regional sustainability, offering a powerful tool to alleviating human–water conflicts, ensuring food security, thereby supporting the region's pathway toward sustainable development. However, the scarcity of regional-scale CHANS models constrains progress in practical applications for regional sustainability. The Yellow River basin (YRB) is an ideal region for

modeling regional CHANS due to its closely coupled human and natural systems, which are stressed by water and ecosystem fragility. Here, we developed the CHANS-SD-YRB model using the System Dynamics approach, integrating 10 sectors essential for modeling human-water interactions of the basin, including five human sectors (Population, Economy, Energy, Food, and Water Demand) and five natural sectors (Water Supply, Sediment, Land, Carbon, and Climate). The model can simulate evolution and feedbacks of the YRB CHANS annually at provincial and sub-basin scales, while conserving hydrological connectivity between sub-basins. The model can accurately reproduce historical CHANS dynamics, achieving strong quantitative agreement with historical data ($R > 0.95$ for human sectors and $R > 0.7$ for natural sectors), which supports its applicability for scenario analyses and future projections. We applied the model to explore human–natural system dynamics under a future baseline scenario, assuming the continuation of existing policies and climate projection under middle of the road scenario (SSP–RCP 2-4.5). The future projections (2021-2100) indicate that achieving sustainable development in the YRB will remain challenging, though economic growth and food security are expected to improve. Emerging issues, such as ecological–human water trade-offs, labor shortages, reduced sediment load, and limited carbon absorption capacity, may hinder regional long-term sustainability.

Keywords: coupled human-natural systems, regional modeling, system dynamics, the Yellow River Basin

1 Introduction

Coupled human and natural systems (CHANS) emphasize the reciprocal feedback and co-evolution between human and natural systems, offering an integrated framework for diagnosing complex problems and guiding sustainable development (Fu and Li, 2016). By capturing dynamic interactions of interconnected components, CHANS theories and models enable more effective policies and interventions that align ecological integrity with socioeconomic progress (Motesharrei et al., 2016; Verburg et al., 2016). Numerous integrated modelling approaches have been developed to simulate

human–natural interactions at the global scale. These include system dynamics-based integrated assessment models (IAMs), such as ANEMI (Breach and Simonovic, 2021), FeliX (Rydzak et al., 2013; Ye et al., 2024), and FRIDA (Rajah et al., 2025), process-based and optimization-based IAMs (Vaidyanathan, 2021), and Earth system models with synchronously coupled human components, such as E3SM-GCAM (Di Vittorio et al., 2025) and integrated Earth system models (iESMs) (Jain et al., 2022). These models effectively characterize human–natural interactions at the global scale, and have been applied to assess the impacts of climate change on human society (e.g., agriculture (Monier et al., 2018), economic damage (Wang et al., 2020b), fatalities increase and welfare loss (Dottori et al., 2018)), and humans' feedback on the Earth system, such as those from climate mitigation on water and food security (Cheng et al., 2022; Fujimori et al., 2022).

Currently, most CHANS models are at the global scale (Calvin and Bond-Lamberty, 2018) with much fewer regional models. While global modeling research has deepened our knowledge of dynamic feedbacks among Earth's spheres and system evolution under climate change, sustainability challenges often manifest at regional scales, where social and ecological dynamics are more intricately intertwined (Liu et al., 2007). Compared to global CHANS, regional CHANS are open systems that continuously exchange energy and materials with other regions and the global system, e.g., water resources and electricity transfers (Dobbs et al., 2023; Zhang et al., 2022a) and trade (Ristaino et al., 2021), resulting in pericoupling and telecoupling of different systems (Liu, 2017). Besides, regional CHANS are shaped by more immediate and complex human influences and stressors, such as urban expansion (van Vliet, 2019), ecological protection (Xu et al., 2017; Yang et al., 2022), and water resource regulation policies (diversion and allocation) (Song et al., 2024), which alter regional CHANS dynamics. Due to their diverse ecological and socioeconomic resilience, regional CHANS exhibit heterogeneous responses to external weather events and climate change, as evidenced by differing responses in crop yield (Hasegawa et al., 2021) and

economic production to extreme heat and warming (Waidelich et al., 2024a). Furthermore, the coarse spatiotemporal resolution of global models limits their capacity to support effective decision-making for regional development (X. Li et al., 2018). As such, advancing regional CHANS modeling is essential for informing adaptive strategies in the face of growing regional environmental and societal pressures.

To address this limitation, many regional CHANS models have been developed at various regional scales (e.g., national, basin, and urban) using System Dynamics (SD) and agent-based modeling (ABMs) techniques. Notable examples include the ANIME-Yangtze model (Jiang et al., 2022), the T21-China (Qu et al., 2020), and the iSDG-Australia model (Allen et al., 2019), all based on SD, the Jordan Water Model (Yoon et al., 2021) with its core on ABM, as well as integrated models in the San Juan River Basin (Hyun et al., 2019) and the Heihe River Basin (Li et al., 2021). These models are designed to capture finer-scale dynamics and region-specific human–natural interactions, since they embed localized characteristics (e.g., fishing ban, reservoir operation strategies, demographic policies, transboundary flows) and account for heterogeneity overlooked by global models. As a result, regional CHANS models offer stronger policy relevance, providing actionable insights for national, basin, and urban decision-making, and advancing CHANS research across multiple scales.

The Yellow River Basin (YRB) in China is one of the regions where conflicts between human and natural systems are most acute and complex, particularly in terms of human–water relations, due to the severe imbalance between socioeconomic development and natural hydrological, ecosystem processes. The YRB faces severe water stress, with the water resource utilization rate exceeding 80% (Feng and Zhu, 2022; Zhang et al., 2022b). Intensive water extraction has triggered a series of ecological and environmental issues, including flow interruptions, water pollution, and declining groundwater levels, all of which in turn constrain socioeconomic development. The Yellow River traverses the Loess Plateau (Zhu et al., 2019), where severe soil erosion makes the Yellow River one of the most sediment-laden rivers

globally (Fu et al., 2011; Yin et al., 2021). The pronounced spatial and temporal variability in streamflow and sediment load leads to significant riverbed aggradation, frequent flooding, and disruption of agricultural production and other livelihood activities (Miao et al., 2016). Due to internal hydrological connectivity, sub-basins are highly interconnected and are susceptible to upstream influences. Upstream water overuse diminishes downstream availability (Wei et al., 2023), a factor that played a major role in flow interruptions during the 1990s (Changming and Shifeng, 2002; Wang et al., 2019). Ecological challenges differ across the subbasin, with the upstream facing ecosystem degradation and limited water retention (Ning et al., 2022), the midstream characterized by soil erosion and large-scale ecological restoration (Fu et al., 2011), and the downstream focusing on wetland conservation (Fu et al., 2023). Policy measures aimed at ecological restoration, such as afforestation and cropland conversion, have increased vegetation cover, reduced sediment loads but also decreased runoff, exacerbating water scarcity (Feng et al., 2016; Wang et al., 2016). These interlinked dynamics underscore the YRB as a complex coupled human–natural system, where addressing environmental challenges requires an integrated, systems-oriented approach.

The existing models for the YRB are typically designed for specific problems with a narrow application focus and only represent a limited set of human and natural components within the CHANS. These include limited nature-to-human impact pathways, e.g., low flows threatening farmers' livelihoods (Liu et al., 2008), the damage of floods and droughts on agriculture (Zhang et al., 2015), as well as human-to-nature impact pathways, e.g., effects of ecological restoration policy on hydropower and water–sediment–carbon dynamics (Wu et al., 2025; Yan et al., 2024), and the impacts of irrigation water-saving and salinity-control practices on crop yield and water productivity (Wu et al., 2023). These models focus on isolated components of CHANS, with limited consideration of fully coupled human–natural interactions, which limits their capacity to represent full human–natural interactions and support regional decision-making.

To address the gap in CHANS modeling for the YRB, following our previously proposed CHANS modeling framework for the basin (Sang et al., 2025b), we implemented the framework to develop the coupled human and natural systems model for the YRB (CHANS-SD-YRB) using the System Dynamics approach. Through dynamic interaction with policies, climate change, human activities, and environmental feedbacks, the CHANS-SD-YRB model provides a platform for predicting system dynamics, conducting scenario analyses, evaluating policies, and optimizing water-food-carbon synergies. This study ~~offers~~presents a detailed description and methodological documentation of the model, offering both theoretical and practical insights ~~for advancing~~to advance regional CHANS modeling and ~~promoting~~promote sustainable development in the YRB.

2 Description of the CHANS-SD-YRB

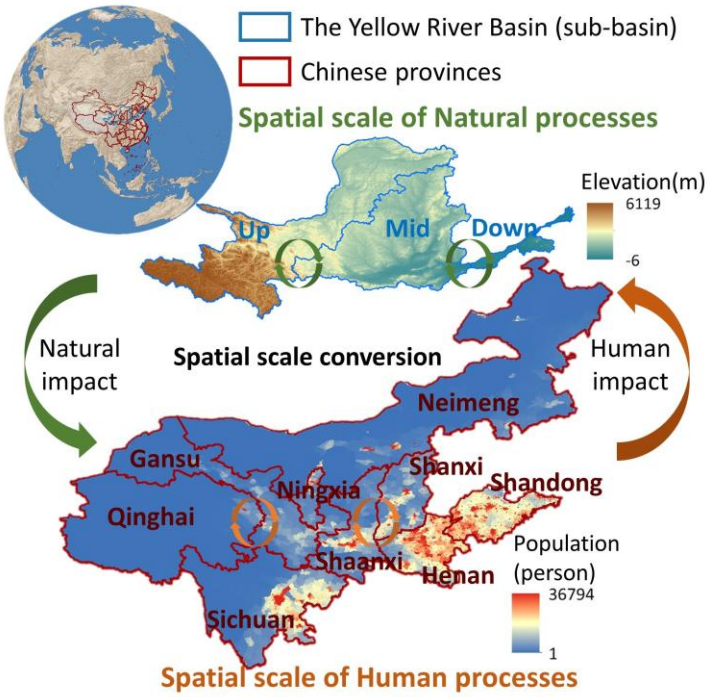

Fig.1 Geolocation of the Yellow River Basin and boundary of the natural and human

processes in the CHANS-SD-YRB model. Natural processes are simulated at the sub-basin scale (base map: elevation), and human processes at the provincial scale across nine provinces (base map: population density in 2020).

We developed the CHANS-SD-YRB based on system dynamics, a method well-suited for capturing complex system behaviors characterized by nonlinearity, multi-level structures, and feedback loops (Forrester, 1968; Richardson, 2011). The model was constructed and implemented using the VENSIM DSS (Ventana Systems, 2023) software platform, operating on an annual time step. The CHANS-SD-YRB simulates both human and natural processes for historical simulations (1981–2020) and future projections (2021–2100). Human processes are simulated at the provincial scale, covering the nine provinces along the Yellow River (Qinghai, Sichuan, Gansu, Ningxia, Neimeng, Shaanxi, Shanxi, Henan, and Shandong), while natural processes are simulated at the sub-basin scale (up-, mid-, and downstream) (Fig.1). The model is designed to capture the various interactions within and between different components of human system and natural system across administrative and hydrological units. The spatial scale conversion between provincial and sub-basin levels relies on weights (e.g., the proportion of sub-basin-level values to provincial total values) derived from historical high-resolution gridded datasets of human-related variables. These weights enable disaggregation of provincial outputs to the sub-basin level (see Supporting Information S4 for details). Given the availability of gridded data for human processes and the strong correlations among relevant variables, gridded population and GDP data were used as proxies to disaggregate demographic variables and economic and human carbon emissions, respectively, from provincial-level to the sub-basin scale (Table S3).

2.1 Model structure

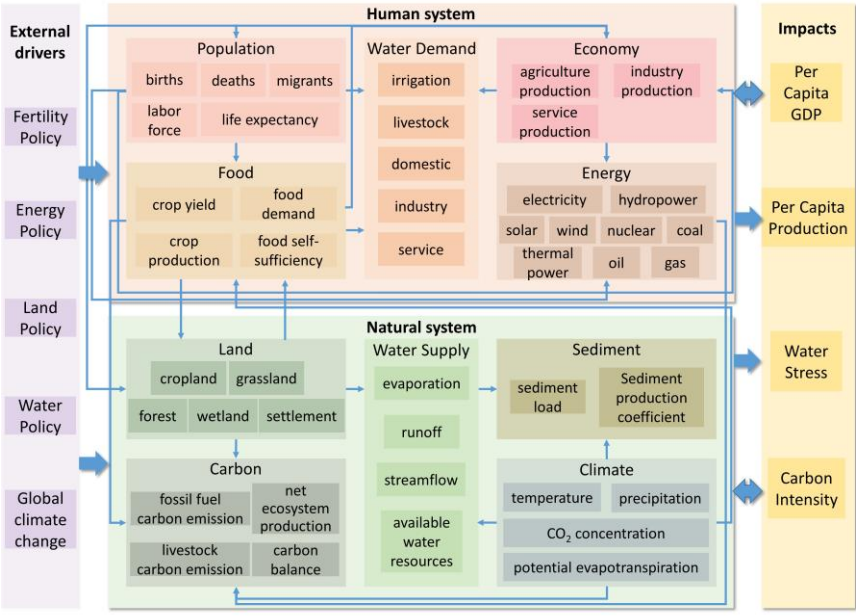

Fig.2 Structure of the CHANS-SD-YRB, which shows sectors of human and natural systems, their key processes and interactions.

Drawing on the modeling framework of CHANS in the YRB (Sang et al., 2025b), we designed the CHANS-SD-YRB structure (Fig. 2), including five sectors related to human society (*Population*, *Economy*, *Energy*, *Food*, and *Water Demand*), and five sectors related to natural ecosystem (*Water Supply*, *Sediment*, *Land*, *Carbon,* and *Climate*).

These sectors are interconnected to represent various human-natural interactions as summarized below. Key interactions among human system modules are summarized below. The *Population* sector affects food demand (*Food*), residential water use (*Water Demand*), household electricity and gas consumption (*Energy*), and settlement land area (*Land*). The sector also interacts dynamically with the *Economy* sector, where economic output influences deaths and migrants, while the labor force, in turn, drives economic production. The *Economy* sector drives energy uses (electricity, coal, oil, and gas use)

from *Energy*, as well as industrial and service water withdrawal from *Water Demand.* The gross agricultural production in the *Economy* is made up of crop and livestock production (*Food*). The *Energy* sector produces fossil fuel emissions in the *Carbon* sector. The *Food* sector is affected by the *Land* and *Climate* sector, and it also determines irrigation water withdrawal (*Water Demand*) and livestock-related emissions (*Carbon*). Additionally, the *Food* sector interacts closely with the *Land* sector, where crop production depends on cropland area, which, in turn, is influenced by food self-sufficiency. The *Water Demand* sector affects streamflow in the *Water Supply* sector through consumptive water use.

The key interactions among natural system modules are listed below. The *Land* sector influences evapotranspiration in the *Water Supply* sector through vegetation coverage, and it influences carbon absorption in *Carbon* sector through land use area. The carbon absorption is also affected by climatic variables including temperature, precipitation, and CO_2 concentration. Similarly, runoff in the *Water Supply* sector is affected by precipitation, precipitation intensity (mm/h, the rate of rainfall within one hour calculated from daily data), and potential evapotranspiration. Streamflow influences sediment dynamics in the *Sediment* sector together with the *Climate* sector.

In addition, the CHANS dynamics in the YRB are modulated by external drivers, including policies and global climate change that affect various modeled processes (e.g., fertility, energy, land use, and water). With comprehensive representation of CHANS processes and their interactions, the CHANS-SD-YRB model is capable of generating integrated indicators to assess the state of the coupled system, such as per capita GDP, per capita food production, water stress, and carbon intensity. These indicators not only serve as evaluation metrics but also feed back to influence the internal dynamics of the human–natural system in the YRB.

2.2 Sector description

The CHANS-SD-YRB model focuses on the essential human–natural processes in the YRB, with a particular emphasis on human–water interactions. To this end, it has a

comprehensive representation of the full range of natural and human processes that influence water use and supply. Formulation of each sector aims to explicitly account for cross-sectoral interactions as fully as possible while remaining sufficiently simple to be implemented within the SD software. Considering data availability and the spatial scales of process, human sectors (*Population*, *Economy*, *Energy*, *Food*, and *Water Demand*) are simulated at the provincial level, while natural sectors (*Water Supply*, *Sediment*, *Land*, *Carbon*, and *Climate*) are simulated at the sub-basin level within the YRB. Next, we describe each sector and its key formulation and provide full details in Supporting Information S2.

2.2.1 Population

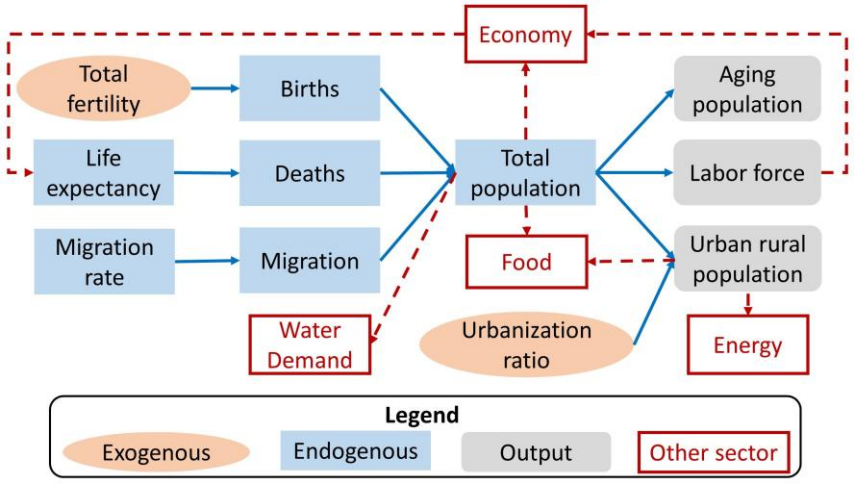

Fig.3 Structure of the *Population* sector. Blue lines indicate connections inside the sector, red dotted lines indicate connections with other sectors.

Population dynamics are driven by births, deaths, and migration (Fig. 3). Births are calculated based on exogenous total fertility rates derived from historical data (Equation S2) to reflect the strong influence of China's Family Planning Policy. Deaths are determined by the life expectancy, which is modeled as a function of human well-being (Equations S3-S6). Migration is calculated based on historical statistical data and per capita GDP differences between YRB and the national average level (Equations S7-

S8). The total population is characterized by age and gender with exogenous urbanization ratios. The output of *Population* sector drives *Economy*, *Energy*, *Food*, and *Water Demand* sectors through labor force, urban and rural populations.

The key variable, total population, is modeled using the age-structured mathematical method (Kemei et al., 2024), which categorizes individuals by one-year age group and gender (Equation 1),

$$Pop_{g,a} = IniPop_{g,a} + \begin{cases} \int \left(B_{g,a} + NM_{g,a} - D_{g,a}\right)dt, & a = 0 \\ \int \left(Pop_{g,a} + NM_{g,a} - D_{g,a}\right)dt, & 1 \le a \le 99, a = 100 \text{ and over} \end{cases} \quad (1)$$

where *Pop* is population, subscript *g* and *a* are gender (g = M is male, g = F is female) and age (a = 0-100 and over); $IniPop_{g,a}$ is the population in the initial year, $B_{g,a}$ is the births, $D_{g,a}$ is the deaths, and $NM_{g,a}$ is the net migrants (i.e., immigrants – emigrations).

2.2.2 Economy

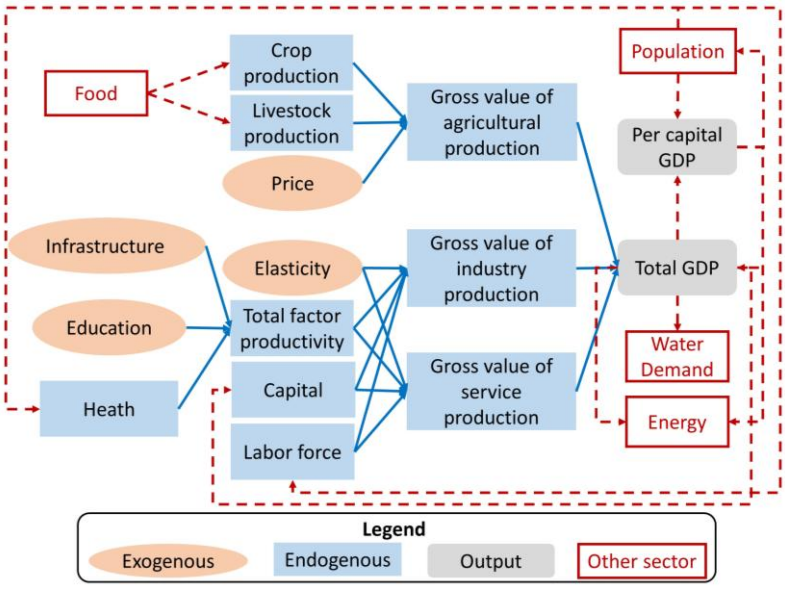

Fig.4 Structure of the *Economy* sector. Blue lines indicate connections inside the sector, red dotted lines indicate connections with other sectors.

The *Economy* sector simulates production activities in agriculture, industry, and

services, which in turn drive changes in the *Population*, *Energy*, and *Water Demand* sectors (Fig. 4).

The gross product of industry and services is calculated using the Cobb-Douglas production function (Cobb and Douglas, 1928) to account for multiple factors in the economy (Equation 2). Exogenous variables (infrastructure, education, and elasticity), and endogenous variables (health and labor force) from the *Population* sector (Equations S10-S21) all affect the gross domestic product in industry and service (GDP_s),

$$GDP_s = IniGDP_s \times TFP_s \times \left(\frac{L_s}{IniL_s}\right)^{1-\alpha_s} \times \left(\frac{K_s}{IniK_s}\right)^{\alpha_s} \quad (2)$$

where subscript s represents industry and service, $IniGDP_s$ is the initial GDP; TFP_s is the total factor productivity calculated from exogenous (infrastructure, education, and elasticity) and endogenous variables (health and labor force) (Equations S10-S13); L_s represents the labor force and $IniL_s$ is its initial value (from *Population* sector); α_s and $1\text{-}\alpha_s$ are capital and labor elasticities from T21-China (Qu et al., 2020) and calibrated using historical data; K_s and $IniK_s$ refer to the capital stock and its initial level.

Gross agricultural production includes crop and livestock production from *Food* sector, calculated by their respective prices (Equations S22-S23).

2.2.3 Energy

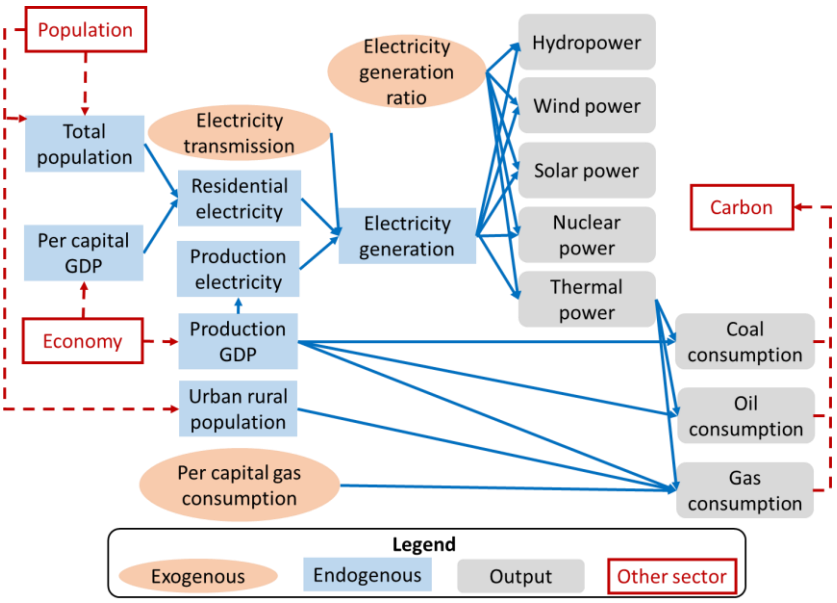

Fig.5 Structure of the *Energy* sector. Blue lines indicate connections inside the sector, red dotted lines indicate connections with other sectors.

The *Energy* sector simulates production, consumption, and the structure of the energy system, encompassing fossil fuels (coal, oil, and gas) and electricity (Fig. 5). Energy production and consumption are always balanced in this sector. Electricity generation is divided into residential and production uses, the former is estimated from the linear fit of historical per capita GDP and residential demand, and the latter is calculated using GDP and electricity intensity data from the China Energy Statistical Yearbook (NBSC, 2020a) (Equations S24-S25). Cross-provincial electricity transmission is also incorporated according to the same yearbook. The shares of electricity generated from thermal, hydro, wind, solar, and nuclear sources are determined by exogenously specified ratios, as reported in the China Energy Statistical Yearbook (NBSC, 2020a). The fossil fuel consumption by economic production of industry and service sectors is modeled as a linear function of sectoral GDP based on historical data (Equations S26-S28). It combines with fossil fuel consumption for

electricity generation and residential gas consumption to drive carbon emissions in the *Carbon* sector.

2.2.4 Food

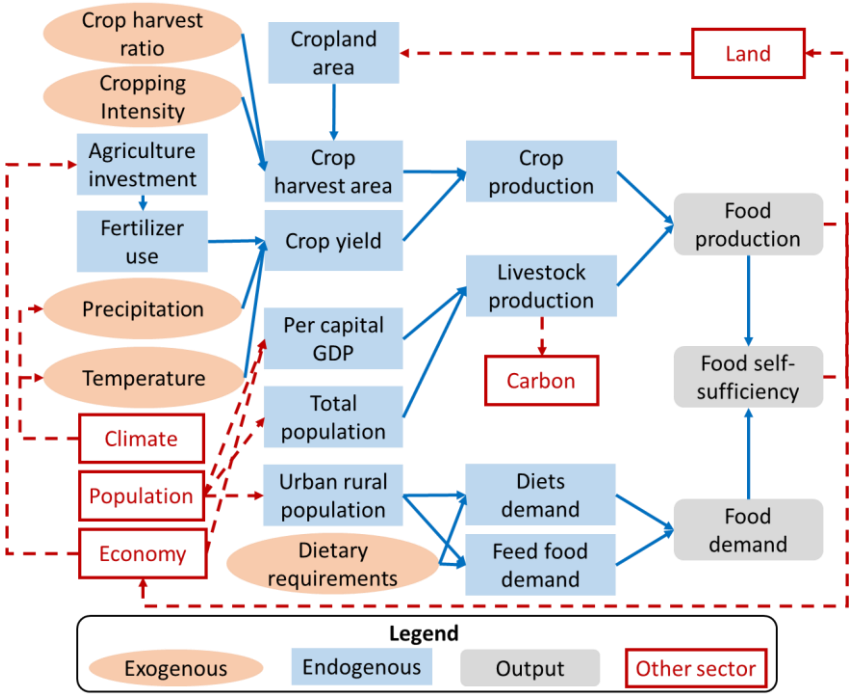

Fig.6 Structure of the *Food* sector. Blue lines indicate connections inside the sector, red dotted lines indicate connections with other sectors.

The *Food* sector simulates the production of livestock and crops, and food demand, and these productions directly affect gross agricultural production in the *Economy* sector (Fig. 6). Livestock production ($Livestock_{pro}$) is calculated by an empirical function, driven by economic development and population growth (Equation 3),

$$Livestock_{pro} = Pop \times \left(Para_{GL1} + (Para_{GL2} - Para_{GL1}) \times \frac{PC_{GDP}}{PC_{GDP}+Const_{GL}}\right) \quad (3)$$

where $Para_{GL1}$、$Para_{GL2}$ and $Const_{GL}$ are parameters obtained by fitting the historical per capita meat production and per capita GDP (PC_{GDP}) data.

Crop production ($Crop_{pro}$) is determined by the yield ($Yield_c$) and harvest area (PA_c) of seven major crop types (subscript c): rice, wheat, corn, soybeans, cotton, potatoes,

and oil crops (Equation 4). The harvest area is influenced by cropland area from the *Land* sector, exogenous cropping intensity and crop harvest ratio. Crop yields are positively affected by agricultural investment from the *Economy* sector, along with effects of precipitation, temperature, and CO_2 concentration from the *Climate* sector (Equations S30-S36).

$$Crop_{pro} = \sum_{c=1}^{7} Yield_c \times PA_c \quad (4)$$

Food demand encompasses both staple and feed grain demand, which are determined by population size from *Population* sector and dietary patterns (Equations S37-S41).

2.2.5 Water Demand

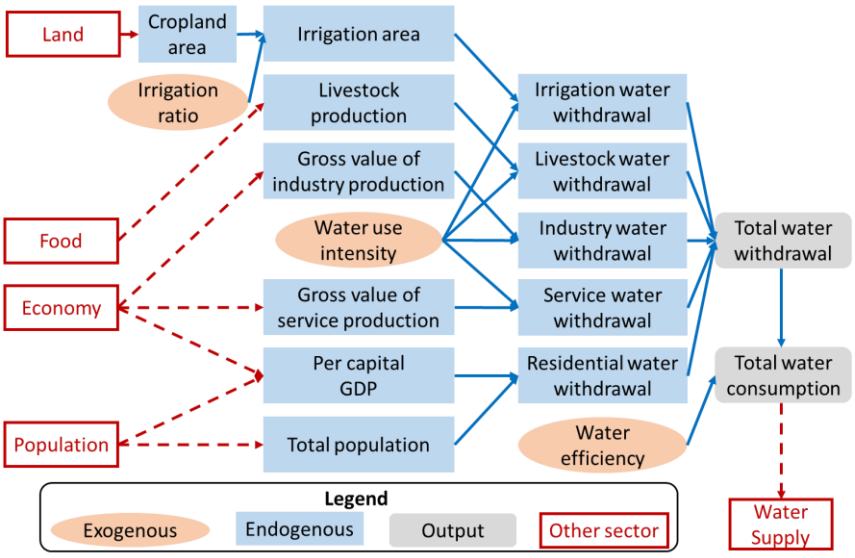

Fig.7 Structure of the *Water Demand* sector. Blue lines indicate connections inside the sector, red dotted lines indicate connections with other sectors.

The *Water Demand* sector simulates water withdrawal (*WW*) and consumption (*WC*) across multiple uses—irrigation, livestock, industry, services, and residential—in the nine provinces of the YRB (Fig. 7). Water consumption is derived as the product of water withdrawal and water use efficiency reported in the Water Resources Bulletin (YRCCMWR, 2020) (Equations S42-S43), which affects the *Water Supply* sector.

Irrigation water withdrawal (WW_{irr}) is estimated through a physically-based function of exogenous irrigation water use intensity (WWI_{irr}), cropland irrigation ratios (IR) from the China Agricultural Yearbook (MAARA, 2020), and cropland area ($Area_{Cropland}$) provided by the *Land* sector (Equation 5).

$$WW_{irr} = WWI_{irr} \times Area_{Cropland} \times IR \quad (5)$$

The water withdrawal for livestock, industry, and services is also driven by exogenous sectoral water use intensities collected from the China Statistical Yearbook and National Long-term Water Use Dataset of China (Zhou et al., 2020), in combination with livestock production from the *Food* sector, economic output from the *Economy* sector (Equations S45-S48).

Residential water withdrawal (WW_{res}) is derived from a non-linear empirical function of economic development and population growth with an upper limit of per capita domestic water use (Flörke et al., 2013) because water demand per person cannot increase indefinitely (Equation 6),

$$WW_{res} = Pop \times \left(Para_{GD1} + (Para_{GD2} - Para_{GD1}) \times \frac{PC_{GDP}}{PC_{GDP} + Const_{GD}}\right) \quad (6)$$

where $Para_{GD1}$, $Para_{GD2}$, and $Const_{GD}$ are parameters obtained by fitting the historical per capita domestic water use with per capita GDP (PC_{GDP}).

2.2.6 Water Supply

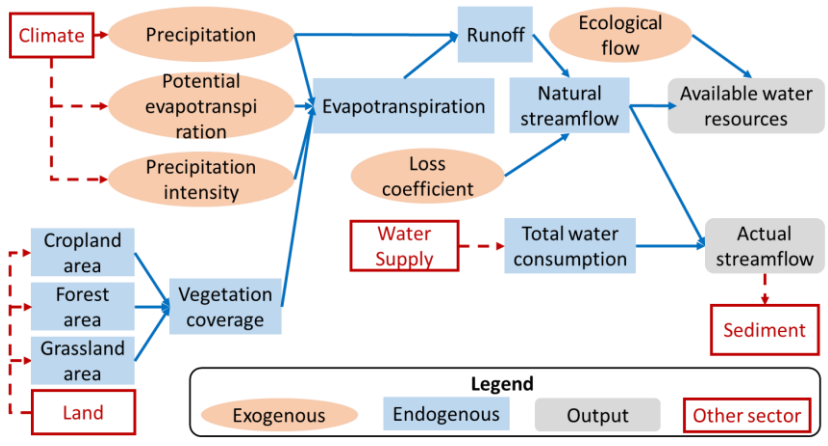

Fig.8 Structure of the *Water Supply* sector. Blue lines indicate connections inside the sector, red dotted lines indicate connections with other sectors.

The *Water Supply* sector simulates runoff, discharge, and their changes in each sub-basin (Fig. 8). Runoff (*R*) is determined by precipitation (*Pre*) and evapotranspiration (*ET*) based on the water balance principle derived from the Budyko equation, which is suitable for non-humid regions of China (Yang et al., 2009) (Equation 7).

$$R = Pre - ET \quad (7)$$

The *ET* is calculated by various exogenous climate variables from the *Climate* sector, and vegetation coverage from the *Land* sector (Equations 8-9, S51-S53),

$$ET = \frac{PET \times Pre}{(Pre^n + EP^n)^{\frac{1}{n}}} \quad (8)$$

$$n = Para_{E1} \times \left(\frac{Ks}{PI}\right)^{Para_{E2}} \times FVC^{Para_{E3}} \times e^{Para_{E4} tan\beta} \quad (9)$$

where *PET* is potential evapotranspiration at sub-basin, from the *Climate* sector; *n* is a parameter reflecting the basin landscape characteristics, related to saturated hydraulic conductivity (*Ks*), precipitation intensity (*PI*), average slope (β), and fraction of vegetation coverage (*FVC*); $Para_{E1}$, $Para_{E2}$, $Para_{E3}$, and $Para_{E4}$ are parameters fitted from historical data.

Runoff and the loss coefficient (defined by the ratio of natural streamflow to runoff) determine the natural streamflow due to the water loss during the confluence process (Equation S54). Natural streamflow and ecological flow constraints define the upper limit of available water resources. By integrating human water consumption from the *Water Demand* sector across sub-basins, the model calculates the actual streamflow (Equations S55-S57). Actual streamflow is transferred through hydrological connectivity from upstream to midstream and then to downstream, ultimately reaching the sea, which governs sediment transport processes within the *Sediment* sector.

2.2.7 Sediment

The *Sediment* sector estimates sediment load (*Sed*) for each sub-basin using an

empirical model in the literature (Yin et al., 2023b), which links actual streamflow from the *Water Supply* sector to sediment transport,

$$Sed = Para_{SS} \times AS + Const_{SS} \quad (10)$$

where $Para_{SS}$ and $Const_{SS}$ are derived from linear fitting of historical hydrological station data on actual streamflow and sediment load.

2.2.8 Land

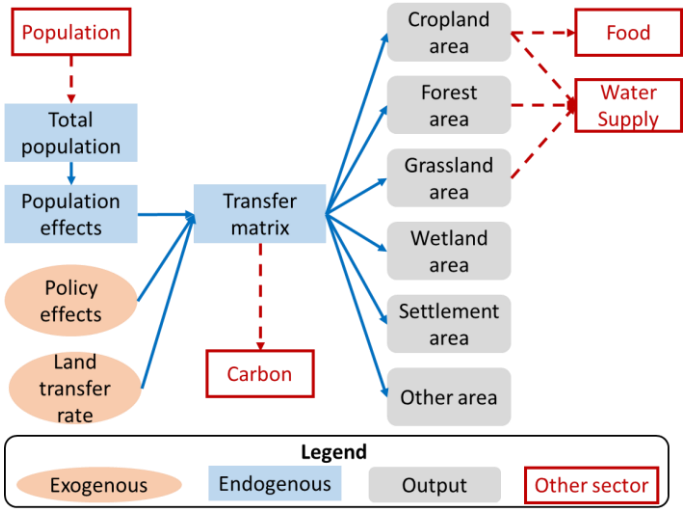

Fig.9 Structure of the *Land* sector. Blue lines indicate connections inside the sector, red dotted lines indicate connections with other sectors.

The *Land* sector simulates the area changes of six land use types (cropland, forest, grassland, wetland, settlement, and others) based on the land transfer matrix obtained from historical remote sensing data (Xu et al., 2018). The land transfer matrix calculates the inflow and outflow of each land category and can be configured to represent the influence of future land use drivers (Fig. 9). This sector outputs vegetation area (including forest, grassland, and cropland), which influences the *Water Supply* sector. Cropland area changes impact the *Food* sector, while land use conversion also plays a role in the *Carbon* sector.

Based on the initial land use area ($IniArea_i$), the transfer matrix determines the area

($Area_i$) allocated to each land use type (Equations 11, S60-S66),

$$Area_i = IniArea_i + \int \left(\sum_{i=1}^{6} FTM_{i,j} - \sum_{j=1}^{6} FTM_{i,j}\right)dt \quad (11)$$

where $FTM_{i,j}$ is the finial land use transfer matrix, indicating the area of land use i transferred to land use j, i and j represent six land use type.

2.2.9 Carbon

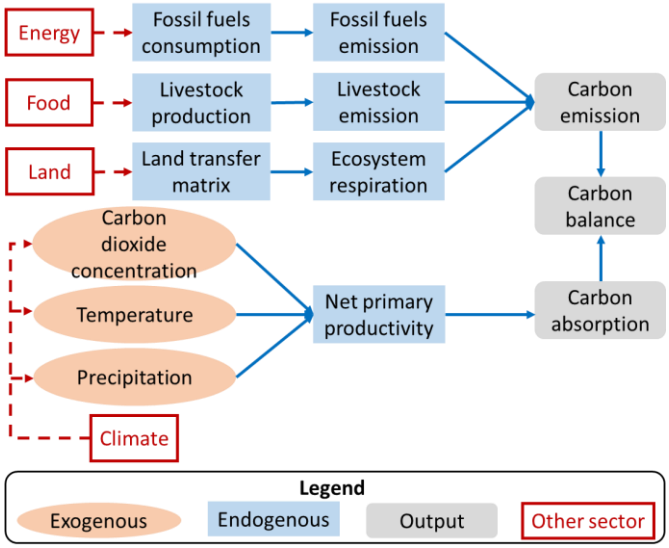

Fig.10 Structure of the *Carbon* sector. Blue lines indicate connections inside the sector, red dotted lines indicate connections with other sectors.

The *Carbon* sector simulates the basin's carbon balance processes, including carbon emission and absorption, adapted from the carbon cycle of ANEMI (Davies and Simonovic, 2011). Carbon emissions (*CE*) encompass fossil fuel emissions, and livestock emission, and ecosystem respiration, which are influenced by outputs from the *Energy*, *Food*, and *Land* sectors (Fig. 10).

Fossil fuel and livestock emissions are calculated based on fossil fuel consumption, livestock production, and their respective emission coefficients. Ecosystem emissions include carbon released from burning as well as from the decomposition of biomass, litter, humus, and charcoal, which are determined by carbon pools' lifespans,

decomposition factor, and respiration coefficients (Equations S67-S93).

Carbon absorption (*CA*) is determined by net primary productivity (*NPP*) and land use area. NPP is influenced by climate factors, including CO_2 concentration, temperature, and precipitation (Equations 12, S63),

$$CA = \sum_{i=1}^{6} NPP_i \times Area_i \quad (12)$$

where i represent land use type, land use area ($Area_i$) from the *Land* sector.

2.2.10 Climate

The *Climate* sector supplies both historical and projected climate data essential for the *Water Supply*, *Food*, and *Carbon* sectors. The key climate variables comprise temperature and precipitation (at the sub-basin and provincial levels), as well as potential evapotranspiration, precipitation intensity, and CO_2 concentration (at the sub-basin level). These variables are treated as exogenous inputs, without accounting for potential feedbacks from human activities or natural system responses on regional climate patterns.

2.3 Data sources

In the model, there are more than 100 exogenous variables, some of which are initial variables that drive the simulation. These exogenous variables are derived either from historical statistical data or from fitted results based on historical data (Table S2). All data sources required for the model simulation are listed in Table 1.

Table 1. Summary of data sources for the YRB model. Updated from Sang et al. (2025).

Sector	Variables*	Data sources	Spatial and temporal scale	Time range
Population	age-specific population, births, deaths, migrants	• China Statistical Yearbook (NBSC, 2020c), • China Population Census Yearbook (NBSC, 2020b)	• provincial, annual	• 1981–2023
Economy	GDP, investment,	• China Agricultural	• provincial,	• 1981–2023

	employment	Yearbook (MAARA, 2020), • China Statistical Yearbook (NBSC, 2020c)	annual	
Energy	electricity, coal, oil, gas consumption	• China Energy Statistical Yearbook (NBSC, 2020a)	• provincial, annual	• 1981–2023
Food	crop production, fertilizer, irrigated area	• China Agricultural Yearbook (MAARA, 2020)	• provincial, annual	• 1981–2023
Water demand	Industrial, domestic, irrigation water withdrawal	• National Long-term Water Use Dataset of China (NLWUD) (Zhou et al., 2020) • China Statistical Yearbook (NBSC, 2020c)	• prefectural, annual	• 1965–2013 • 1981–2023
Water supply	runoff, streamflow, water stress	• China Natural Runoff Dataset (CNRD) (Gou et al., 2021), • Gauge-based Natural Streamflow Dataset (Miao et al., 2022) • Yellow River Water Resources Bulletin (YRCCMWR, 2020)	• 0.25° grid, Monthly • 0.25° grid, annual • provincial, annual	• 1961–2018 • 1961–201 域代码已更改 • 1998–2022
Sediment	sediment load	• Yellow River Water Resources Bulletin (YRCCMWR, 2020)	• provincial, annual	• 1998–2022
Land	cropland, forest, grassland, wetland, settlement	• China land use remote sensing monitoring dataset (CNLUCC) (Xu et al., 2018) • Long-term global land surface satellite fractional vegetation cover product (Jia et al., 2015, 2019)	• 1 km grid, annual	• 1980, 1990, 1995, 2000, 2005, 2010, 2015, 2020
Carbon	fossil fuel carbon emissions, net	• Carbon Emission Accounts and Datasets	• Provincial, annual	• 1997–2021 • 1981–2018

	primary productivity	• (Shan et al., 2018), Global Vegetation Productivity Products (GVPP) (Cui et al., 2016; Wang et al., 2020a; Yu et al., 2018)	• 5 km grid, 8 day		
Climate	temperature, precipitation, CO_2 concentration, potential evapotranspiration and precipitation intensity	• Gridded daily observation dataset over China region (Wu and Gao, 2013), • European Environment Agency (EEA, 2019), • China Meteorological Data Service Center (https://data.cma.cn/)	• 0.25° grid, Annual • Global, Annual • Meteorological stations, Monthly	• 1961–2020 • 1800-2020 • 1956-2018	

425 * Listed are some typical variables of each sector

426 ## 3 Model validation and application

427 ### 3.1 Historical model validation

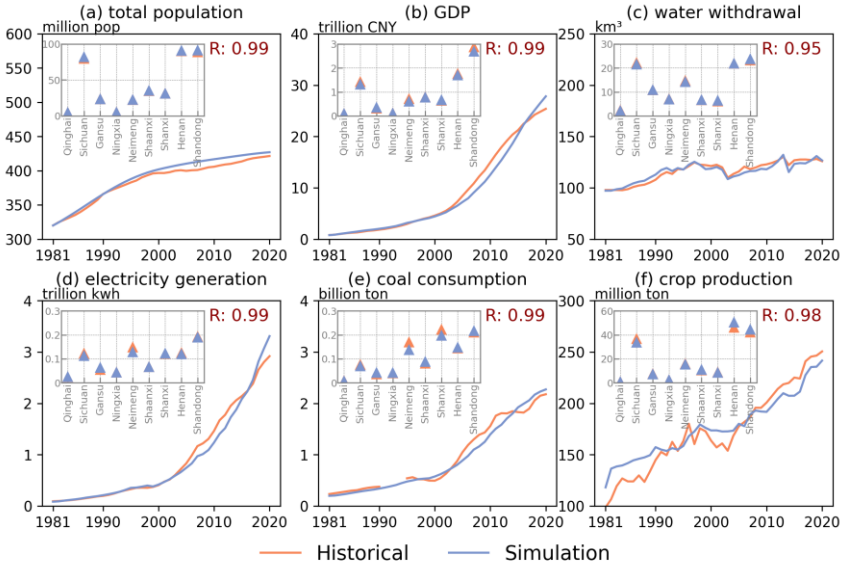

428

429 Fig.11 Validation of human system processes during historical period of 1981-2020.

430 (a) total population in *Population* sector; (b) GDP in *Economy* sector; (c) water

431 withdrawal in *Water Demand* sector; (d) electricity generation and (e) coal

consumption in *Energy* sector; (f) crop production in *Food* sector. Pink triangles in the upper left sub-image represents the average of historical and simulation value in 1981-2020 of each province in the YRB.

We compared model performance during the historical period (1981–2020) against historical data. These data are sourced from multiple channels, including statistical yearbooks, hydrological stations, remote sensing observations, and outputs from other models (Table S3).

For human sectors, the simulation accuracy of selected key variables from each sector is consistently high ($R > 0.95$), including total population, gross domestic product (GDP), water withdrawal, electricity generation, coal consumption, and crop production across the nine provinces (Fig.11). However, the accuracy varies among provinces, particularly for GDP, electricity generation, coal consumption, and crop production. Some provinces, like Neimeng, exhibit lower simulation accuracy for certain indicators than others, probably due to the simplification of relevant modelled processes, imperfect parameterizations, and external policy interventions. Among all sectors, the greatest uncertainty arises in simulating coal consumption, because the absence of a clear historical trend results in poor fitting performance. Nevertheless, the model performs reasonably well in the human sectors, effectively capturing the historical dynamics of human systems in the YRB.

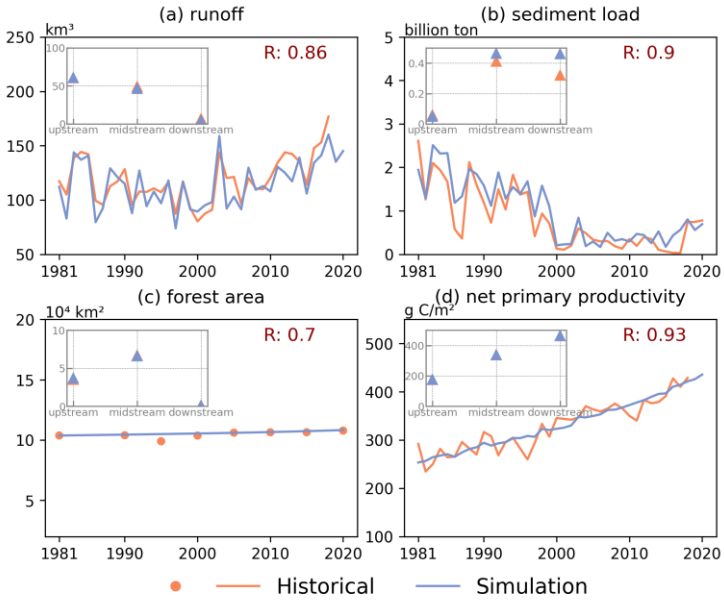

Fig.12 Validation of the natural system processes during historical period of 1981-2020. (a) runoff in *Water Supply* sector; (b) sediment load in *Sediment* sector; (c) forest area in *Land* sector, and the historical dataset is discontinuous; (d) net primary productivity in *Carbon* sector. Pink triangles in the upper left sub-image represents the average of historical and simulation value in 1981-2020 of each sub-basin in the YRB.

For natural sectors, the simulation accuracy for runoff, sediment load, forest area, and NPP in the YRB is relatively high ($R > 0.7$) (Fig.12). At the sub-basin level, the overall performance is satisfactory; however, the model shows lower accuracy in simulating sediment transport in the mid- and downstream. Compared to the human sectors, the natural sectors generally exhibit lower correlations with historical data, largely due to the simplifications required when modeling physically complex natural processes. Nevertheless, the model is still capable of capturing the historical dynamics of natural processes in the YRB.

Sensitivity analyses with randomly generated parameter values reveal growing

uncertainty in the long-term trajectories of socio-economic and natural variables; the model maintains behavioral robustness across all runs without catastrophic collapse or unrealistic oscillations (see Supporting Information S3 for details).

3.2 Model application for future projection

3.2.1 Future baseline scenario

The future baseline scenario represents a trajectory in which existing plans and policies continue to operate without substantial changes in external environments. The development of the baseline scenario primarily relies on variables from the *Population*, *Economy*, *Water Demand*, and *Land* sector based on available government planning documents, historical trends, and other projections (Table 2). For future projections, variables or parameters not specified in the table are held constant at historical levels from their most recent year. Future climate data (2015-2100) are from the ensemble mean of 11 CMIP6 models (ACCESS-CM2, CESM2, CMCC-ESM2, GFDL-ESM4, INM-CM4-8, INM-CM5-0, IPSL-CM6A-LR, MIROC6, MRI-ESM2-0, UKESM1-0-LL, and HadGEM-GC31-LL) (available at https://cds.climate.copernicus.eu/datasets/projections-cmip6?tab=download) for the SSP 2-4.5 because this scenario aligns more closely with the climate trends in the YRB. To ensure temporal consistency, CMIP6 historical climate data (1981–2014) were used instead of observed historical records. To reduce systemic biases in the raw CMIP6 data, we applied bias correction using CN05 and ground weather stations observations from 1981 to 2014. By statistically aligning the mean of the CMIP6 data with observation records, systemic bias is removed while retaining the temporal consistency required for long-term simulation.

We run the model under the future baseline scenario to project the evolution of CHANS in the basin from 2021 to 2100 (see Supporting Information S6 for details of future scenario design and supplementary spreadsheet for exogenous variables).

Table 2 Settings of key variables in the future baseline scenario

Sector	Variables	Future baseline

Population	• Total fertility • Gender ratio • Average years of schooling • Urban and rural population ratio • Labor force	• 2024 United Nations Population Projections • 2024 United Nations Population Projections • The national maximum in 2023 (Germany) as the upper limit • Analysis and Forecast of Urbanization Trends in China's Modernization by 2020 • Delay retirement age
Energy	• Electricity generation sources ratio • Irrigation intensity	• Projected provincial-level energy structure meeting China’s carbon peaking and carbon neutrality goals (Li et al., 2024) • Irrigation water use intensity declines linearly (1%/yr) to its minimum value.
Water Demand	• Industry, service, livestock water use intensity	• Industry, service and livestock water use intensity declines linearly (1%/yr) to its minimum value.
Land	• Land use area	• Cropland, forest, and grassland are allowed to be converted into each other, but not to unused land; unused land can be converted to the rest land; wetlands are fixed. • Minimum cropland area above the red line for cropland protection.
Climate	• Temperature • Precipitation • Potential evapotranspiration • Precipitation intensity • CO_2 concentration,	• SSP 2-4.5 —— CMIP 6

3.2.2 Projection of CHANS dynamics in future baseline scenario

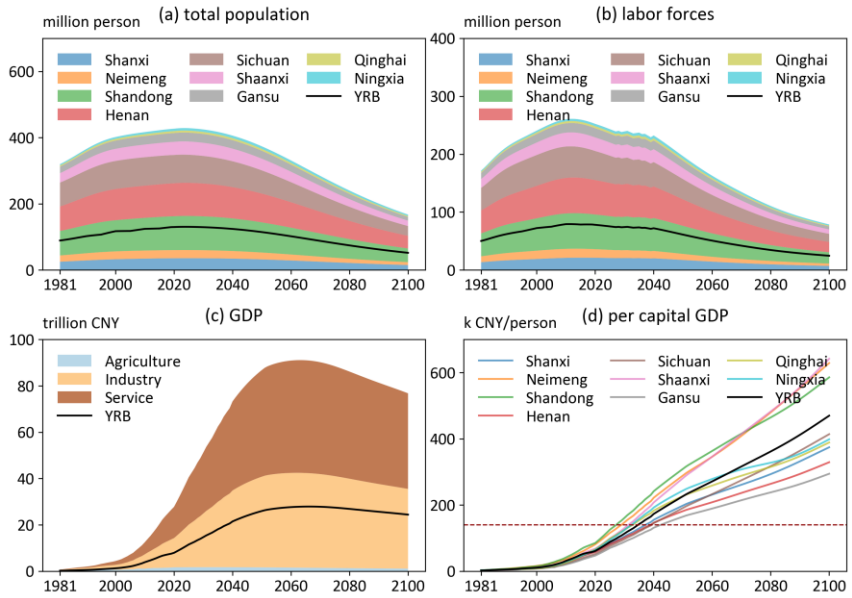

Fig.13 Changes in key variables of the *Population* and *Economy* sector in the future baseline scenario: (a) the total population, (b) the total labor forces, (c) the gross output of agriculture, industry, and service, and the total gross domestic output, (d) the per capita GDP in nine provinces and YRB.

The model simulates human and natural system dynamics under the future baseline scenario and produces outputs for nine provinces and their corresponding areas within the YRB. The simulation results are reported either at the provincial level (nine provinces) for human system sectors or at the basin level (basin boundary) for natural system sectors. The total population in the nine provinces and the YRB is projected to peak in 2023 and 2024, at 429 million and 131 million, respectively, driven by declining fertility rates (Fig.13 (a)). The labor force peaks earlier, reaching 261 million in the nine provinces in 2012 and 79 million in the YRB in 2011 (Fig.13 (b)). After 2025, the labor force is projected to increase again due to the delayed retirement policy. GDP in the nine provinces is expected to increase until a peak in 2063, at 91 trillion CNY (three

times the 2020 level, in 2020 constant prices), under the influence of a labor force decline, with the YRB reaching its peak four years later (Fig.13 (c)). In contrast to total GDP, per capita GDP in all regions is projected to continue rising throughout the future period (Fig.13 (d)). Although all provinces demonstrate improvements in economic status and living standards, considerable regional disparities persist. Among the nine provinces, Shaanxi demonstrates the largest growth in average per capita GDP from 2021 to 2100 relative to the historical period (1981-2020), with a more than seventeenfold increase, while the YRB as a whole shows an over thirteenfold increase.

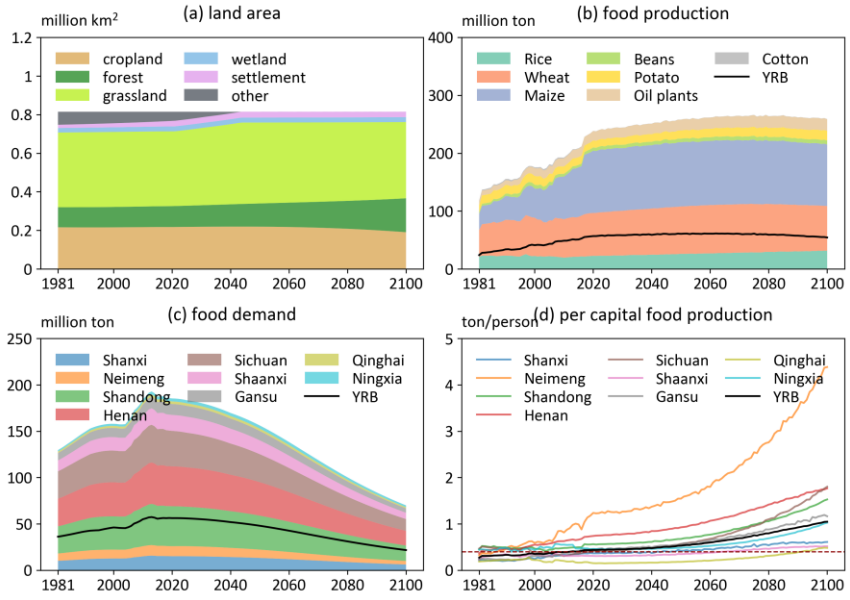

Fig.14 Land and food in the future baseline scenario. (a) land area in the YRB; (b-d) food production of seven crop types, food demand and per capita food production in nine provinces and the YRB, red dotted line represents the 0.4 tons international food security threshold.

Under the future baseline scenario, land use patterns remain relatively stable based on historical trends~~,~~ (Fig. 14(a)), as no new land use policies are introduced and cropland area in each province has to stay above ~~the red line (a~~a mandatory minimum

~~cropland area for each province~~ threshold for food security~~) (Fig.14 (a)).~~ (China's Cropland Red Line policy). The forest area is projected to increase gradually, reaching 62% above the 2021 level by 2100, while the cropland area is expected continue declining, falling 12% below the 2021 level. Total crop production in nine provinces and YRB is projected to peak in 2079 and 2062 (Fig.14 (b)), respectively, driven by the combined effects of declining cropland area and increasing crop yields. Food demand in both the nine provinces and the YRB as a whole peaked in 2013 (193 million tons and 57 million tons, respectively) (Fig.14 (c)), largely driven by population dynamics. In the future, per capita food production in the YRB is projected to consistently exceed the international food security threshold of 0.4 tons per person (Fig.14 (d)). However, in certain years, provinces such as Qinghai and Shaanxi could fall below this standard.

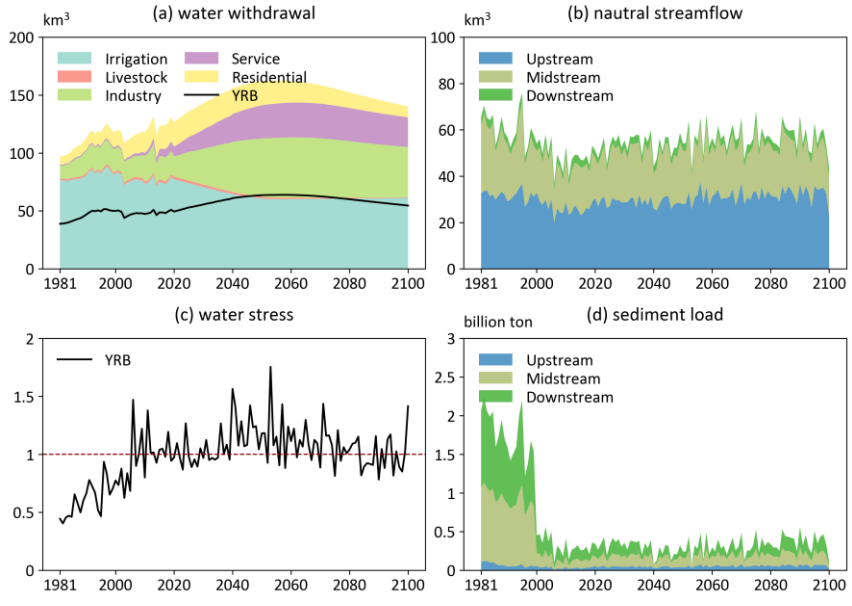

Fig.15 Water demand and supply in the future baseline scenario. (a) water withdrawal across five water-use sectors in nine provinces and the YRB; (b) natural streamflow in up-, mid- and downstream; (c) water stress in the YRB, red dotted line represents the water security threshold; (d) sediment load in the up-, mid- and downstream.

Total water withdrawal in the nine provinces and the YRB is projected to peak in 2056 and 2058, reaching 162 km³ and 64 km³, respectively (Fig.15 (a)). Irrigation water withdrawal is expected to decline, driven by reductions in cropland area and irrigation intensity, the latter resulting from improvements in irrigation efficiency assumed in the scenario. Peaks in residential, industrial, service, and livestock water withdrawals are primarily associated with projected peaks in population and GDP. Natural streamflow is projected to exhibit a fluctuating upward trend of 0.073 km³/year basin-wide (Fig. 15(b)), with the most significant growth in the upstream region (0.068 km³/year). Considering the ecological flow requirement of 18.7 km^3 (YRCCMWR, 2015), water stress (calculated as water consumption divided by (natural discharge - ecological flow)) is expected to decline in the latter half of the century, largely due to the peak and subsequent reduction in water withdrawal. However, overall water stress is projected to exceed historical levels in 2041 and will fall below 1 in 38% of the years (Fig.15 (c)), reflecting persistent human–water tensions and future trade-offs between ecological and human water use. As a result of reduced actual streamflow, sediment transport in the Yellow River is projected to decline sharply (Fig.15 (d)), with a 71% decrease in sediment load relative to the historical period.

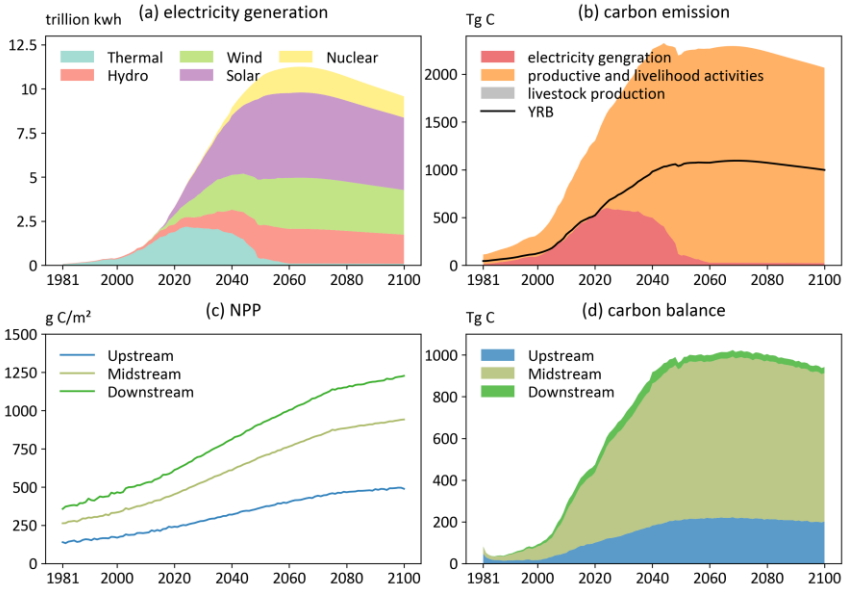

Fig.16 Electricity and carbon in the future baseline scenario. (a) the electricity generation from five sources in nine provinces; (b) carbon emission from three sources in nine provinces and the YRB; (c-d) the net primary productivity and carbon balance in the up-, mid-, and downstream.

Since the energy system is transitioning to carbon neutrality goals under the future baseline scenario, thermal power generation is projected to decline sharply, while clean energy (hydropower, wind, solar, and nuclear) will become the dominant source for electricity generation (Fig.16 (a)). The large-scale adoption of clean energy will lead to a peak in carbon emissions from electricity generation in 2024 (Fig.16 (b)). In contrast, emissions from productive and livelihood activities are projected to rise substantially over time, with total human emissions in the YRB reaching a peak in 2044. NPP is anticipated to increase markedly in response to CO_2 concentration increase (Fig.16 (c)). Although the carbon balance of the YRB has remained positive (net carbon source), it is expected to gradually decline after 2068 (Fig.16 (d)), indicating that the basin's ecosystems alone cannot fully offset human-induced carbon emissions.

The above projections of future baseline scenarios highlight persistent challenges

to achieving sustainable development in the YRB, underscoring the need for integrated policy responses to address these challenges. Priority should be given to enhancing water-use efficiency and establishing adaptive water resource allocation mechanisms that balance ecological and human water needs. Sediment management strategies, which combine ecological restoration with hydraulic regulation, are necessary to maintain river stability and delta health. To counter the decline in labor force, policies should promote industrial upgrading and technological innovation. Strengthening the basin's carbon mitigation capacity requires accelerating the clean energy transition and expanding ecological restoration to enhance carbon sequestration. Finally, a multi-sectoral, CHANS-based governance framework should be established to coordinate water, land, energy, and carbon management, enabling evidence-based scenario analysis and adaptive policy design for long-term sustainability.

4 Discussion and conclusions

The development of the CHANS-SD-YRB model involves a series of key considerations in translating a conceptual framework into a functioning model. The framework focuses on human–water interactions in the YRB, integrating bidirectional feedback between human and natural processes. SD was chosen to implement the framework, as it effectively captures feedback, non-linear relationships, and cross-sectoral linkages within complex human–natural systems, while remaining practical and straightforward to use. For quantitative representation of human–natural processes, we prefer theoretical methods that incorporate key interactions within the system suitable for implementation using SD. For example, the Budyko framework connects the *Land*, *Climate*, *Water Demand*, and *Water Supply* sectors. Relative to distributed hydrological models, it offers lower computational complexity and reduced data requirements. The Cobb–Douglas production function links the *Population* and *Economy* sectors. Compared with Computable General Equilibrium models (Fujimori et al., 2014a), it is simpler to construct and requires fewer parameters and data inputs. When no suitable theoretical framework/method is available to describe a process, we

rely on empirical relationships derived from historical data. For example, crop yields are estimated using fitted relationships between climate variables, fertilizer application, and historical yields. For processes that cannot be represented through empirical functions, we apply literature-based estimates to obtain approximate quantitative relationships, such as fossil fuel emission factors. For processes influenced by external drivers that cannot be endogenously expressed within the model, we quantify them using exogenous parameters derived from historical statistics, such as water intensity. Given the heterogeneous human–natural interactions in the YRB, we represent all processes at the provincial and sub-basin scales using scale-specific parameters, except where parameters or data at these levels are unavailable.

The CHANS-SD-YRB model explicitly couples multiple human and natural sectors, enabling a more integrated representation of feedbacks across population, economy, energy, food, water, sediment, land, carbon, and climate. Unlike models that focus on specific sectors or isolated subsystems—such as eco-hydrological models and sediment transport models, which may well capture individual processes but cannot represent the complex human–nature interactions driving system dynamics. Our model's integration of human and natural sectors provides a robust framework for addressing regional CHANS challenges and offers practical guidance for sustainable development. The CHANS-SD-YRB model serves as a comprehensive platform for conducting system dynamics prediction, scenario analysis, policy evaluation, and optimization, to alleviate human–water conflicts, ensure food security, and achieve long-term sustainability. For example, analysis of the impacts of the 1987 Yellow River water allocation policy (Song et al., 2024) offer valuable insights for adjusting interprovincial water distribution to promote sustainable water governance; assessment of ecological restoration policies (Li et al., 2015) can guide future ecological engineering; spatiotemporal dynamics of future water gaps can serve as a valuable reference for planning inter-basin water transfers. The model's flexibility also allows for the incorporation of additional feedback, for example, linking water scarcity to

industrial output or climate warming to agricultural productivity. These could include the effects of global warming on human health (Yin et al., 2023a) and economic activities (Nordhaus, 2017), water constraints on production, dietary shifts influencing carbon emissions and land use (Ren et al., 2023), and the trade-offs between carbon mitigation and food security (Xu et al., 2022).

Nevertheless, the model remains subject to further refinement. The current simplifications of natural processes could be replaced with more sophisticated models to enhance simulation accuracy. For instance, the YRB hydrological processes involve highly complex human interventions, including reservoir, conservation, and revegetation projects (Wang et al., 2025). The refined runoff simulations by distributed hydrological models improve water supply assessments through their better characterization of spatial heterogeneity in soil, precipitation, and snowmelt (Cong et al., 2009). For human processes, the *Energy* and *Economy* sectors could be refined to model more detailed industry subsectors and emerging trends in energy demand driven by electrification. Given the uncertainty in future climate change, the sensitivity of the system's future projections to alternative climate change scenarios (SSP1-2.6, SSP3-7.0, or SSP5-8.5) warrants exploration. Moreover, there are still important feedbacks absent from the current coupling framework. Notable examples include the effects of land use change on climate, the effects of climate change on economic growth, and the effects of pricing on energy use and carbon emissions. These missing feedbacks could be incorporated based on recent studies, including the land use feedback on precipitation through moisture recycling (Sang et al., 2025a), socioeconomic losses from impacts of climate change and extremes (Waidelich et al., 2024b), and integration with Computable General Equilibrium (CGE) models (Fujimori et al., 2014b). In particular, recent modeling work by Wells et al. (2026) demonstrated that a more comprehensive representation of climate-to-society feedbacks is possible within the system dynamics framework. Additionally, the model's spatial and temporal resolutions are relatively coarse due to the inherent mismatch in spatiotemporal scales between

human and natural processes. The scale at which we make the model represents a practical compromise, constrained by data availability and aligned with the study's objectives. Simulations at finer scales (e.g., monthly, daily, or gridded) would enhance the representation of natural processes (e.g., hydrological processes, land use changes, and food production) and the associated spatiotemporal heterogeneity (e.g., daily simulations can assess the impacts of extreme weather). However, it may also exacerbate the scale mismatch with socioeconomic processes, making it challenging to analyze cross-sectoral dynamics. Technically, the inherent limitations of the SD software restrict the model's ability to represent temporal fluctuations and spatial variations. To overcome this, transitioning from the VENSIM platform to a code-based implementation will be necessary, which would also facilitate coupling with other models. Future research should prioritize these improvements to strengthen both the performance and applicability of the model.

Drawing on the conceptual framework of Sang et al. (2025), this study implements it into a fully functional, validated System Dynamics model tool, CHANS-SD-YRB 1.0. The model fills the gap in CHANS modeling for the YRB. It integrates the dynamics of ten interconnected sectors: *Population*, *Economy*, *Energy*, *Food*, *Water Demand*, *Water Supply*, *Sand*, *Land*, *Carbon*, and *Climate*, achieving reciprocal feedback between human and natural systems. This model can serve as a robust tool to inform policy decisions that influence the evolution of coupled human–natural systems and to explore pathways for optimizing these systems toward sustainability. Furthermore, the modeling process provides valuable experience for regional CHANS modeling and contributes to advancing the broader development of CHANS models at the regional scale.

Code and data availability

The CHANS-SD-YRB V1.0 model (Vensim DSS format), along with the input data and simulation outputs used in this study, are openly accessible at https://doi.org/10.5281/zenodo.17568962 (Sang, 2025), and

https://github.com/sangshan-ss/CHANS_SD_YRB.

Author contributions

Conceptualization: YL, SS[1], BF. Data curation: SS[1]. Formal analysis: SS[1]. Funding acquisition: BF, YL. Investigation: YL, SS[1]. Methodology: SS[1], YL, BF. Project administration: YL. Resources: YL. Software: SS[1], SZ, LY. Supervision: YL, BF. Validation: SS[1], SZ, LY. Visualization: SS[1]. Writing – original draft: SS[1]. Writing – review and editing: SS[1], YL, SW, YXL, XTW, SS[2], WZ, XHW. (Note: SS[1] refers to Shan Sang, and SS[2] refers to Shuang Song, to distinguish between authors with identical initials.)

Competing interests

The authors declare that they have no conflict of interest.

Acknowledgements

We thank Dr. Weishuang Qu for developing the Threshold 21 model in the Millennium Institute that inspired this study, and also for his and Dr. Haiyan Jiang's generous help with the CHANS-SD-YRB modeling. We also thank the data support from Dr. Xianghui Kong, and National Earth System Science Data Center, National Science & Technology Infrastructure of China (http://www.geodata.cn).

Financial support

This study is supported by the National Natural Science Foundation of China (Grant No. 42041007), and the Fundamental Research Funds for the Central Universities.

References:

Allen, C., Metternicht, G., Wiedmann, T., and Pedercini, M.: Greater gains for Australia by tackling all SDGs but the last steps will be the most challenging, Nat Sustain, 2, 1041–1050, https://doi.org/10.1038/s41893-019-0409-9, 2019.

Breach, P. A. and Simonovic, S. P.: ANEMI3: An updated tool for global change analysis, PLoS ONE, 16, e0251489, https://doi.org/10.1371/journal.pone.0251489, 2021.

Calvin, K. and Bond-Lamberty, B.: Integrated human-earth system modeling—state of

717 the science and future directions, Environ. Res. Lett., 13, 063006,
718 https://doi.org/10.1088/1748-9326/aac642, 2018.

719 Changming, L. and Shifeng, Z.: Drying up of the yellow river: its impacts and counter-
720 measures, Mitigation and Adaptation Strategies for Global Change, 7, 203–214,
721 https://doi.org/10.1023/A:1024408310869, 2002.

722 Cheng, Y., Huang, M., Lawrence, D. M., Calvin, K., Lombardozzi, D. L., Sinha, E.,
723 Pan, M., and He, X.: Future bioenergy expansion could alter carbon sequestration
724 potential and exacerbate water stress in the United States, Science Advances, 8,
725 eabm8237, https://doi.org/10.1126/sciadv.abm8237, 2022.

726 Cobb, C. W. and Douglas, P. H.: A theory of production, The American Economic
727 Review, 18, 139–165, 1928.

728 Cong, Z., Yang, D., Gao, B., Yang, H., and Hu, H.: Hydrological trend analysis in the
729 Yellow River basin using a distributed hydrological model, Water Resources Research,
730 45, 2008WR006852, https://doi.org/10.1029/2008WR006852, 2009.

731 Cui, T., Wang, Y., Sun, R., Qiao, C., Fan, W., Jiang, G., Hao, L., and Zhang, L.:
732 Estimating Vegetation Primary Production in the Heihe River Basin of China with
733 Multi-Source and Multi-Scale Data, PLOS ONE, 11, e0153971,
734 https://doi.org/10.1371/journal.pone.0153971, 2016.

735 Davies, E. G. R. and Simonovic, S. P.: ANEMI: a new model for integrated assessment
736 of global change, Interdisciplinary Environmental Review, 2011.

737 Di Vittorio, A. V., Sinha, E., Hao, D., Singh, B., Calvin, K. V., Shippert, T., Patel, P.,
738 and Bond-Lamberty, B.: E3SM-GCAM: A Synchronously Coupled Human Component
739 in the E3SM Earth System Model Enables Novel Human-Earth Feedback Research,
740 Journal of Advances in Modeling Earth Systems, 17, e2024MS004806,
741 https://doi.org/10.1029/2024MS004806, 2025.

742 Dobbs, G. R., Liu, N., Caldwell, P. V., Miniat, C. F., Sun, G., Duan, K., and Bolstad, P.
743 V.: Inter-basin surface water transfers database for public water supplies in
744 conterminous United States, 1986–2015, Sci Data, 10, 255,
745 https://doi.org/10.1038/s41597-023-02148-5, 2023.

746 Dottori, F., Szewczyk, W., Ciscar, J.-C., Zhao, F., Alfieri, L., Hirabayashi, Y., Bianchi,
747 A., Mongelli, I., Frieler, K., Betts, R. A., and Feyen, L.: Increased human and economic
748 losses from river flooding with anthropogenic warming, Nature Clim Change, 8, 781–
749 786, https://doi.org/10.1038/s41558-018-0257-z, 2018.

750 EEA: Trends in atmospheric concentrations of CO2 (ppm), CH4 (ppb) and N2O (ppb),
751 between 1800 and 2017, 2019.

752 Feng, X., Fu, B., Piao, S., Wang, S., Ciais, P., Zeng, Z., Lü, Y., Zeng, Y., Li, Y., Jiang,
753 X., and Wu, B.: Revegetation in China's Loess Plateau is approaching sustainable water
754 resource limits, Nature Clim Change, 6, 1019–1022,
755 https://doi.org/10.1038/nclimate3092, 2016.

756 Feng, Y. and Zhu, A.: Spatiotemporal differentiation and driving patterns of water
757 utilization intensity in Yellow River Basin of China: Comprehensive perspective on the
758 water quantity and quality, Journal of Cleaner Production, 369, 133395,
759 https://doi.org/10.1016/j.jclepro.2022.133395, 2022.

760 Flörke, M., Kynast, E., Bärlund, I., Eisner, S., Wimmer, F., and Alcamo, J.: Domestic
761 and industrial water uses of the past 60 years as a mirror of socio-economic
762 development: A global simulation study, Global Environmental Change, 23, 144–156,
763 https://doi.org/10.1016/j.gloenvcha.2012.10.018, 2013.

764 Forrester, J. W.: Principles of systems, Pegasus Communications, Inc, Waltham, MA,
765 1968.

766 Fu, B. and Li, Y.: Bidirectional coupling between the Earth and human systems is
767 essential for modeling sustainability, National Science Review, 3, 397–398,
768 https://doi.org/10.1093/nsr/nww094, 2016.

769 Fu, B., Liu, Y., Lü, Y., He, C., Zeng, Y., and Wu, B.: Assessing the soil erosion control
770 service of ecosystems change in the Loess Plateau of China, Ecological Complexity, 8,
771 284–293, https://doi.org/10.1016/j.ecocom.2011.07.003, 2011.

772 Fu, B., Liu, Y., and Meadows, M. E.: Ecological restoration for sustainable
773 development in China, National Science Review, 10, nwad033,
774 https://doi.org/10.1093/nsr/nwad033, 2023.

775 Fujimori, S., Masui, T., and Matsuoka, Y.: Development of a global computable general
776 equilibrium model coupled with detailed energy end-use technology, Applied Energy,
777 128, 296–306, https://doi.org/10.1016/j.apenergy.2014.04.074, 2014a.

778 Fujimori, S., Masui, T., and Matsuoka, Y.: Development of a global computable general
779 equilibrium model coupled with detailed energy end-use technology, Applied Energy,
780 128, 296–306, https://doi.org/10.1016/j.apenergy.2014.04.074, 2014b.

781 Fujimori, S., Wu, W., Doelman, J., Frank, S., Hristov, J., Kyle, P., Sands, R., van Zeist,
782 W.-J., Havlik, P., Domínguez, I. P., Sahoo, A., Stehfest, E., Tabeau, A., Valin, H., van
783 Meijl, H., Hasegawa, T., and Takahashi, K.: Land-based climate change mitigation
784 measures can affect agricultural markets and food security, Nat Food, 3, 110–121,
785 https://doi.org/10.1038/s43016-022-00464-4, 2022.

786 Gou, J., Miao, C., Samaniego, L., Xiao, M., Wu, J., and Guo, X.: CNRD v1.0: A High-

787 Quality Natural Runoff Dataset for Hydrological and Climate Studies in China, Bulletin
788 of the American Meteorological Society, 102, E929–E947,
789 https://doi.org/10.1175/BAMS-D-20-0094.1, 2021.

790 Hasegawa, T., Sakurai, G., Fujimori, S., Takahashi, K., Hijioka, Y., and Masui, T.:
791 Extreme climate events increase risk of global food insecurity and adaptation needs,
792 Nat Food, 2, 587–595, https://doi.org/10.1038/s43016-021-00335-4, 2021.

793 Hyun, J.-Y., Huang, S.-Y., Yang, Y.-C. E., Tidwell, V., and Macknick, J.: Using a
794 coupled agent-based modeling approach to analyze the role of risk perception in water
795 management decisions, Hydrology and Earth System Sciences, 23, 2261–2278,
796 https://doi.org/10.5194/hess-23-2261-2019, 2019.

797 Jain, S., Mindlin, J., Koren, G., Gulizia, C., Steadman, C., Langendijk, G. S., Osman,
798 M., Abid, M. A., Rao, Y., and Rabanal, V.: Are We at Risk of Losing the Current
799 Generation of Climate Researchers to Data Science?, AGU Advances, 3,
800 e2022AV000676, https://doi.org/10.1029/2022AV000676, 2022.

801 Jia, K., Liang, S., Liu, S., Li, Y., Xiao, Z., Yao, Y., Jiang, B., Zhao, X., Wang, X., Xu,
802 S., and Cui, J.: Global Land Surface Fractional Vegetation Cover Estimation Using
803 General Regression Neural Networks From MODIS Surface Reflectance, IEEE
804 Transactions on Geoscience and Remote Sensing, 53, 4787–4796,
805 https://doi.org/10.1109/TGRS.2015.2409563, 2015.

806 Jia, K., Yang, L., Liang, S., Xiao, Z., Zhao, X., Yao, Y., Zhang, X., Jiang, B., and Liu,
807 D.: Long-Term Global Land Surface Satellite (GLASS) Fractional Vegetation Cover
808 Product Derived From MODIS and AVHRR Data, IEEE Journal of Selected Topics in
809 Applied Earth Observations and Remote Sensing, 12, 508–518,
810 https://doi.org/10.1109/JSTARS.2018.2854293, 2019.

811 Jiang, H., Simonovic, S. P., and Yu, Z.: ANEMI_Yangtze v1.0: a coupled human–
812 natural systems model for the Yangtze Economic Belt – model description, Geosci.
813 Model Dev., 26, 2022.

814 Kemei, Z., Rotich, T., and Bitok, J.: Modelling population dynamics using age-
815 structured system of partial differential equations, IJAMR, 13, 110–116,
816 https://doi.org/10.14419/m81azj37, 2024.

817 Li, M., Shan, R., Abdulla, A., Virguez, E., and Gao, S.: The role of dispatchability in
818 China's power system decarbonization, Energy Environ. Sci., 17, 2193–2205,
819 https://doi.org/10.1039/D3EE04293F, 2024.

820 Li, X., Cheng, G., Lin, H., Cai, X., Fang, M., Ge, Y., Hu, X., Chen, M., and Li, W.:
821 Watershed System Model: The Essentials to Model Complex Human-Nature System at

the River Basin Scale, Journal of Geophysical Research: Atmospheres, 123, 3019–3034, https://doi.org/10.1002/2017JD028154, 2018.

Li, X., Zhang, L., Zheng, Y., Yang, D., Wu, F., Tian, Y., Han, F., Gao, B., Li, H., Zhang, Y., Ge, Y., Cheng, G., Fu, B., Xia, J., Song, C., and Zheng, C.: Novel hybrid coupling of ecohydrology and socioeconomy at river basin scale: A watershed system model for the Heihe River basin, Environmental Modelling & Software, 141, 105058, https://doi.org/10.1016/j.envsoft.2021.105058, 2021.

Li, Z., Liu, X., Niu, T., Kejia, D., Zhou, Q., Ma, T., and Gao, Y.: Ecological Restoration and Its Effects on a Regional Climate: The Source Region of the Yellow River, China, Environ. Sci. Technol., 49, 5897–5904, https://doi.org/10.1021/es505985q, 2015.

Liu, C., Golding, D., and Gong, G.: Farmers' coping response to the low flows in the lower Yellow River: A case study of temporal dimensions of vulnerability, Global Environmental Change, 18, 543–553, https://doi.org/10.1016/j.gloenvcha.2008.09.002, 2008.

Liu, J.: Integration across a metacoupled world, E&S, 22, art29, https://doi.org/10.5751/ES-09830-220429, 2017.

Liu, J., Dietz, T., Carpenter, S. R., Alberti, M., Folke, C., Moran, E., Pell, A. N., Deadman, P., Kratz, T., Lubchenco, J., Ostrom, E., Ouyang, Z., Provencher, W., Redman, C. L., Schneider, S. H., and Taylor, W. W.: Complexity of Coupled Human and Natural Systems, Science, 317, 1513–1516, https://doi.org/10.1126/science.1144004, 2007.

MAARA: China Agriculture Yearbook, https://data.cnki.net/yearBook?type=type&code=A, 2020.

Miao, C., Kong, D., Wu, J., and Duan, Q.: Functional degradation of the water–sediment regulation scheme in the lower Yellow River: Spatial and temporal analyses, Science of The Total Environment, 551–552, 16–22, https://doi.org/10.1016/j.scitotenv.2016.02.006, 2016.

Miao, C., Gou, J., Fu, B., Tang, Q., Duan, Q., Chen, Z., Lei, H., Chen, J., Guo, J., Borthwick, A. G. L., Ding, W., Duan, X., Li, Y., Kong, D., Guo, X., and Wu, J.: High-quality reconstruction of China's natural streamflow, Science Bulletin, 67, 547–556, https://doi.org/10.1016/j.scib.2021.09.022, 2022.

Monier, E., Paltsev, S., Sokolov, A., Chen, Y.-H. H., Gao, X., Ejaz, Q., Couzo, E., Schlosser, C. A., Dutkiewicz, S., Fant, C., Scott, J., Kicklighter, D., Morris, J., Jacoby, H., Prinn, R., and Haigh, M.: Toward a consistent modeling framework to assess multi-sectoral climate impacts, Nat Commun, 9, 1–8, https://doi.org/10.1038/s41467-018-

857 02984-9, 2018.

858 Motesharrei, S., Rivas, J., Kalnay, E., Asrar, G. R., Busalacchi, A. J., Cahalan, R. F.,
859 Cane, M. A., Colwell, R. R., Feng, K., Franklin, R. S., Hubacek, K., Miralles-Wilhelm,
860 F., Miyoshi, T., Ruth, M., Sagdeev, R., Shirmohammadi, A., Shukla, J., Srebric, J.,
861 Yakovenko, V. M., and Zeng, N.: Modeling sustainability: population, inequality,
862 consumption, and bidirectional coupling of the Earth and Human Systems, National
863 Science Review, 3, 470–494, https://doi.org/10.1093/nsr/nww081, 2016.

864 NBSC: China Energy Statistical Yearbook,
865 https://data.cnki.net/yearBook?type=type&code=A, 2020a.

866 NBSC: China Population Census Yearbook,
867 https://data.cnki.net/yearBook?type=type&code=A, 2020b.

868 NBSC: China Statistical Yearbooks, https://www.stats.gov.cn/english/, 2020c.

869 Ning, X., Zhu, N., Liu, Y., and Wang, H.: Quantifying impacts of climate and human
870 activities on the grassland in the Three-River Headwater Region after two phases of
871 Ecological Project, Geography and Sustainability, 3, 164–176,
872 https://doi.org/10.1016/j.geosus.2022.05.003, 2022.

873 Nordhaus, W. D.: Revisiting the social cost of carbon, Proceedings of the National
874 Academy of Sciences, 114, 1518–1523, https://doi.org/10.1073/pnas.1609244114,
875 2017.

876 Qu, W., Shi, W., Zhang, J., and Liu, T.: T21 China 2050: A Tool for National Sustainable
877 Development Planning, Geography and Sustainability, 1, 33–46,
878 https://doi.org/10.1016/j.geosus.2020.03.004, 2020.

879 Rajah, J. K., Blanz, B., Kopainsky, B., and Schoenberg, W.: An endogenous modelling
880 framework of dietary behavioural change in the fully coupled human-climate FRIDA
881 v2.1 model, Geoscientific Model Development, 18, 5997–6022,
882 https://doi.org/10.5194/gmd-18-5997-2025, 2025.

883 Ren, M., Huang, C., Wu, Y., Deppermann, A., Frank, S., Havlík, P., Zhu, Y., Fang, C.,
884 Ma, X., Liu, Y., Zhao, H., Chang, J., Ma, L., Bai, Z., Xu, S., and Dai, H.: Enhanced
885 food system efficiency is the key to China's 2060 carbon neutrality target, Nat Food, 4,
886 552–564, https://doi.org/10.1038/s43016-023-00790-1, 2023.

887 Richardson, G. P.: Reflections on the foundations of system dynamics, System
888 Dynamics Review, 27, 219–243, https://doi.org/10.1002/sdr.462, 2011.

889 Ristaino, J. B., Anderson, P. K., Bebber, D. P., Brauman, K. A., Cunniffe, N. J., Fedoroff,
890 N. V., Finegold, C., Garrett, K. A., Gilligan, C. A., Jones, C. M., Martin, M. D.,

MacDonald, G. K., Neenan, P., Records, A., Schmale, D. G., Tateosian, L., and Wei, Q.: The persistent threat of emerging plant disease pandemics to global food security, Proceedings of the National Academy of Sciences, 118, e2022239118, https://doi.org/10.1073/pnas.2022239118, 2021.

Rydzak, F., Obersteiner, M., Kraxner, F., Fritz, S., and McCallum, I.: FeliX3–Impact Assessment Model: Systemic View across Societal Benefit Areas beyond Global Earth Observation, Laxenburg: International Institute for Applied Systems Analysis (IIASA), 2013.

Sang, S.: CHANS-SD-YRB V1.0: A System Dynamics model of the coupled human-natural systems for the Yellow River Basin (1.0.0), https://doi.org/10.5281/zenodo.17568963, 2025.

Sang, S., Li, Y., Hou, C., Zi, S., and Lin, H.: The interprovincial green water flow in China and its teleconnected effects on the social economy, Hydrol. Earth Syst. Sci., 29, 67–84, https://doi.org/10.5194/hess-29-67-2025, 2025a.

Sang, S., Li, Y., Zong, S., Yu, L., Wang, S., Liu, Y., Wu, X., Song, S., Wang, X., and Fu, B.: The modeling framework of the coupled human and natural systems in the Yellow River Basin, Geography and Sustainability, 6, 100294, https://doi.org/10.1016/j.geosus.2025.100294, 2025b.

Shan, Y., Guan, D., Zheng, H., Ou, J., Li, Y., Meng, J., Mi, Z., Liu, Z., and Zhang, Q.: China CO2 emission accounts 1997–2015, Sci Data, 5, 170201, https://doi.org/10.1038/sdata.2017.201, 2018.

Song, S., Wen, H., Wang, S., Wu, X., Cumming, G. S., and Fu, B.: Quantifying the effects of institutional shifts on water governance in the Yellow River Basin: A social-ecological system perspective, Journal of Hydrology, 629, 130638, https://doi.org/10.1016/j.jhydrol.2024.130638, 2024.

Vaidyanathan, G.: Integrated assessment climate policy models have proven useful, with caveats, Proc. Natl. Acad. Sci. U.S.A., 118, e2101899118, https://doi.org/10.1073/pnas.2101899118, 2021.

Ventana Systems, Inc.: Vensim DSS (version 9.3), 2023.

Verburg, P. H., Dearing, J. A., Dyke, J. G., Leeuw, S. van der, Seitzinger, S., Steffen, W., and Syvitski, J.: Methods and approaches to modelling the Anthropocene, Global Environmental Change, 39, 328–340, https://doi.org/10.1016/j.gloenvcha.2015.08.007, 2016.

van Vliet, J.: Direct and indirect loss of natural area from urban expansion, Nat Sustain, 2, 755–763, https://doi.org/10.1038/s41893-019-0340-0, 2019.

926 Waidelich, P., Batibeniz, F., Rising, J., Kikstra, J. S., and Seneviratne, S. I.: Climate
927 damage projections beyond annual temperature, Nat. Clim. Chang., 14, 592–599,
928 https://doi.org/10.1038/s41558-024-01990-8, 2024a.

929 Waidelich, P., Batibeniz, F., Rising, J., Kikstra, J. S., and Seneviratne, S. I.: Climate
930 damage projections beyond annual temperature, Nat. Clim. Chang., 14, 592–599,
931 https://doi.org/10.1038/s41558-024-01990-8, 2024b.

932 Wang, M., Sun, R., Zhu, A., and Xiao, Z.: Evaluation and Comparison of Light Use
933 Efficiency and Gross Primary Productivity Using Three Different Approaches, Remote
934 Sensing, 12, 1003, https://doi.org/10.3390/rs12061003, 2020a.

935 Wang, S., Fu, B., Piao, S., Lü, Y., Ciais, P., Feng, X., and Wang, Y.: Reduced sediment
936 transport in the Yellow River due to anthropogenic changes, Nature Geosci, 9, 38–41,
937 https://doi.org/10.1038/ngeo2602, 2016.

938 Wang, S., Song, S., Zhang, H., Yu, L., Jiao, C., Li, C., Wu, X., Zhao, W., Best, J.,
939 Roberts, P., and Fu, B.: Anthropogenic impacts on the Yellow River Basin, Nat Rev
940 Earth Environ, 6, 656–671, https://doi.org/10.1038/s43017-025-00718-2, 2025.

941 Wang, T., Teng, F., and Zhang, X.: Assessing global and national economic losses from
942 climate change: a study based on CGEM-IAM in China, Clim. Change Econ., 11,
943 2041003, https://doi.org/10.1142/S2010007820410031, 2020b.

944 Wang, Y., Zhao, W., Wang, S., Feng, X., and Liu, Y.: Yellow River water rebalanced by
945 human regulation, Sci Rep, 9, 9707, https://doi.org/10.1038/s41598-019-46063-5, 2019.

946 Wei, Z., Jian, Z., Sun, Y., Pan, F., Han, H., Liu, Q., and Mei, Y.: Ecological sustainability
947 and high-quality development of the Yellow River Delta in China based on the
948 improved ecological footprint model, Sci Rep, 13, 3821,
949 https://doi.org/10.1038/s41598-023-30896-2, 2023.

950 Wells, C. D., Blanz, B., Ramme, L., Breier, J., Callegari, B., Muralidhar, A., Rajah, J.
951 K., Lindqvist, A. N., Eriksson, A. E., Schoenberg, W. A., Köberle, A. C., Wang-
952 Erlandsson, L., Mauritzen, C., Grimeland, M. B., and Smith, C.: The representation of
953 climate impacts in the FRIDAv2.1 Integrated Assessment Model, Geoscientific Model
954 Development, 19, 1229–1260, https://doi.org/10.5194/gmd-19-1229-2026, 2026.

955 Wu, J. and Gao, X.: Agridded daily observation dataset over China region and
956 comparison with the other datasets, Chinese Journal of Geophysics, 56, 1102–1111,
957 https://doi.org/10.6038/cjg20130406, 2013.

958 Wu, X., Yan, Z., Yang, H., Wang, S., Zhang, H., Shen, Y., Song, S., Liu, Y., Guo, Y.,
959 Yang, D., and Fu, B.: Ecological restoration in the Yellow River Basin enhances
960 hydropower potential, Nat Commun, 16, 2566, https://doi.org/10.1038/s41467-025-

57891-7, 2025.

Wu, Z., Li, Y., Wang, R., Xu, X., Ren, D., Huang, Q., Xiong, Y., and Huang, G.: Evaluation of irrigation water saving and salinity control practices of maize and sunflower in the upper Yellow River basin with an agro-hydrological model based method, Agricultural Water Management, 278, 108157, https://doi.org/10.1016/j.agwat.2023.108157, 2023.

Xu, S., Wang, R., Gasser, T., Ciais, P., Peñuelas, J., Balkanski, Y., Boucher, O., Janssens, I. A., Sardans, J., Clark, J. H., Cao, J., Xing, X., Chen, J., Wang, L., Tang, X., and Zhang, R.: Delayed use of bioenergy crops might threaten climate and food security, Nature, 609, 299–306, https://doi.org/10.1038/s41586-022-05055-8, 2022.

Xu, W., Xiao, Y., Zhang, J., Yang, W., Zhang, L., Hull, V., Wang, Z., Zheng, H., Liu, J., Polasky, S., Jiang, L., Xiao, Y., Shi, X., Rao, E., Lu, F., Wang, X., Daily, G. C., and Ouyang, Z.: Strengthening protected areas for biodiversity and ecosystem services in China, Proc. Natl. Acad. Sci. U.S.A., 114, 1601–1606, https://doi.org/10.1073/pnas.1620503114, 2017.

Xu, X., Liu, J., Zhang, S., Li, R., Yan, C., and Wu, S.: China land use remote sensing monitoring dataset, https://doi.org/10.12078/2018070201, 2018.

Yan, Z., Wang, T., Ma, T., and Yang, D.: Water-carbon-sediment synergies and trade-offs: Multi-faceted impacts of large-scale ecological restoration in the Middle Yellow River Basin, Journal of Hydrology, 634, 131099, https://doi.org/10.1016/j.jhydrol.2024.131099, 2024.

Yang, D., Shao, W., Yeh, P. J.-F., Yang, H., Kanae, S., and Oki, T.: Impact of vegetation coverage on regional water balance in the nonhumid regions of China, Water Resources Research, 45, https://doi.org/10.1029/2008WR006948, 2009.

Yang, Z., Li, Q., Xue, W., and Xu, Z.: Impacts of nature reserves on local residents' income in China, Ecological Economics, 199, 107494, https://doi.org/10.1016/j.ecolecon.2022.107494, 2022.

Ye, Q., Liu, Q., Swamy, D., Gao, L., Moallemi, E. A., Rydzak, F., and Eker, S.: FeliX 2.0: An integrated model of climate, economy, environment, and society interactions, Environmental Modelling & Software, 179, 106121, https://doi.org/10.1016/j.envsoft.2024.106121, 2024.

Yin, P., Gao, Y., Chen, R., Liu, W., He, C., Hao, J., Zhou, M., and Kan, H.: Temperature-related death burden of various neurodegenerative diseases under climate warming: a nationwide modelling study, Nat Commun, 14, 8236, https://doi.org/10.1038/s41467-023-44066-5, 2023a.

Yin, S., Gao, G., Ran, L., Lu, X., and Fu, B.: Spatiotemporal Variations of Sediment Discharge and In-Reach Sediment Budget in the Yellow River From the Headwater to the Delta, Water Resources Research, 57, e2021WR030130, https://doi.org/10.1029/2021WR030130, 2021.

Yin, S., Gao, G., Ran, L., Li, D., Lu, X., and Fu, B.: Extreme streamflow and sediment load changes in the Yellow River Basin: Impacts of climate change and human activities, Journal of Hydrology, 619, 129372, https://doi.org/10.1016/j.jhydrol.2023.129372, 2023b.

Yoon, J., Klassert, C., Selby, P., Lachaut, T., Knox, S., Avisse, N., Harou, J., Tilmant, A., Klauer, B., Mustafa, D., Sigel, K., Talozi, S., Gawel, E., Medellín-Azuara, J., Bataineh, B., Zhang, H., and Gorelick, S. M.: A coupled human–natural system analysis of freshwater security under climate and population change, Proceedings of the National Academy of Sciences, 118, e2020431118, https://doi.org/10.1073/pnas.2020431118, 2021.

YRCCMWR: Yellow River Basin Comprehensive Planning (2012-2030), 2015.

YRCCMWR: Yellow River Water Resources Bulletin, 2020.

Yu, T., Sun, R., Xiao, Z., Zhang, Q., Liu, G., Cui, T., and Wang, J.: Estimation of Global Vegetation Productivity from Global LAnd Surface Satellite Data, Remote Sensing, 10, 327, https://doi.org/10.3390/rs10020327, 2018.

Zhang, H., Li, R., Cai, X., Zheng, C., Liu, L., Liu, M., Zhang, Q., Lin, H., Chen, L., and Wang, X.: Do electricity flows hamper regional economic–environmental equity?, Applied Energy, 326, 120001, https://doi.org/10.1016/j.apenergy.2022.120001, 2022a.

Zhang, Q., Gu, X., Singh, V. P., Kong, D., and Chen, X.: Spatiotemporal behavior of floods and droughts and their impacts on agriculture in China, Global and Planetary Change, 131, 63–72, https://doi.org/10.1016/j.gloplacha.2015.05.007, 2015.

Zhang, T., Su, X., Zhang, G., Wu, H., and Liu, Y.: Projections of the characteristics and probability of spatially concurrent hydrological drought in a cascade reservoirs area under CMIP6, Journal of Hydrology, 613, 128472, https://doi.org/10.1016/j.jhydrol.2022.128472, 2022b.

Zhou, F., Bo, Y., Ciais, P., Dumas, P., Tang, Q., Wang, X., Liu, J., Zheng, C., Polcher, J., Yin, Z., Guimberteau, M., Peng, S., Ottle, C., Zhao, X., Zhao, J., Tan, Q., Chen, L., Shen, H., Yang, H., Piao, S., Wang, H., and Wada, Y.: Deceleration of China's human water use and its key drivers, Proceedings of the National Academy of Sciences, 117, 7702–7711, https://doi.org/10.1073/pnas.1909902117, 2020.

Zhu, Y., Jia, X., Qiao, J., and Shao, M.: What is the mass of loess in the Loess Plateau

of China?, Science Bulletin, 64, 534–539, https://doi.org/10.1016/j.scib.2019.03.021, 2019.